GDCh

Research Articles

Angewandte
Chemie
International Edition
www.angewandte.org

Heterogeneous Catalysis

Fundamental Structural and Electronic Understanding of Palladium Catalysts on Nitride and Oxide Supports

Junhao Huang, Marcus Klahn, Xinxin Tian, Stephan Bartling, Anna Zimina, Martin Radtke, Nils Rockstroh, Pawel Naliwajko, Norbert Steinfeldt, Tim Peppel, Jan-Dierk Grunwaldt, Andrew J. Logsdail, Haijun Jiao, and Jennifer Strunk*

Abstract: The nature of the support can fundamentally affect the function of a heterogeneous catalyst. For the novel type of isolated metal atom catalysts, sometimes referred to as single-atom catalysts, systematic correlations are still rare. Here, we report a general finding that Pd on nitride supports (non-metal and metal nitride) features a higher oxidation state compared to that on oxide supports (non-metal and metal oxide). Through thorough oxidation state investigations by X-ray absorption spectroscopy (XAS), X-ray photoelectron spectroscopy (XPS), CO-DRIFTS, and density functional theory (DFT) coupled with Bader charge analysis, it is found that Pd atoms prefer to interact with surface hydroxyl group to form a $Pd(OH)_x$ species on oxide supports, while on nitride supports, Pd atoms incorporate into the surface structure in the form of $Pd-N$ bonds. Moreover, a correlation was built between the formal oxidation state and computational Bader charge, based on the periodic trend in electronegativity.

Introduction

Understanding how the support influences the reactivity of single-atom catalysts (SACs) remains a challenge. The support, to some extent, resembles the organic ligands in a homogeneous complex, and the ligands dictate the electronic properties and reactivity of the metal center.[1] Recent work done by Muravev et al. on cerium dioxide (CeO_2)-supported Pd SACs proved that the size of CeO_2 support governs the reactivity of isolated Pd species in CO oxidation.[2] Another work by Hulva et al. on $Fe_3O_4(001)$-supported SACs demonstrated that the local geometry of metal atoms to the support strongly affects their electronic structure and their interaction with reactants.[3] In those cases, modulating the coordination environment of the metal atom on the support can significantly alter its oxidation state, electronic structure, and steric configuration, thereby regulating overall catalytic properties.

The effect of support type on the electronic structure of SACs has not yet been thoroughly studied in a systematic manner. Among the various types of supported SACs catalysts, those based on nitride and oxide supports have attracted particular attention.[4] For example, TiO_2-supported isolated Pd catalysts have been discovered for the reverse water-gas shift (rWGS) reaction,[5] NO removal,[6] and CO_2 hydrogenation.[7] On the oxide surface, the abundant defect sites (steps, corners, vacancies), lattice O atoms, and hydroxyl groups can serve as anchoring sites for isolated metal atoms.[8] At elevated temperatures, the metal species may even be built into the surface or restructure the surface.[9] Numerous nitride-supported and MOFs-derived carbon-nitrogen-supported Pd SACs have also been developed and studied.[10] For example, polymeric carbon nitride (PCN) supported isolated Pd catalysts exhibit excellent activity and stability for the Suzuki–Miyaura coupling

[*] J. Huang, M. Klahn, S. Bartling, N. Rockstroh, P. Naliwajko,
N. Steinfeldt, T. Peppel, H. Jiao, J. Strunk
Leibniz Institute for Catalysis e.V., Albert-Einstein-Straße 29a, 18059
Rostock, Germany
E-mail: jennifer.strunk@catalysis.de

X. Tian
Institute of Molecular Science, Key Laboratory of Materials for
Energy Conversion and Storage of Shanxi Province, Key Laboratory
of Chemical Biology and Molecular Engineering of Education
Ministry, Shanxi University, Taiyuan 030006, China

A. Zimina, J.-D. Grunwaldt
Institute of Catalysis Research and Technology and Institute for
Chemical Technology and Polymer Chemistry, Karlsruhe Institute of
Technology (KIT), Karlsruhe, Germany

M. Radtke
Federal Institute for Materials Research and Testing (BAM),
Richard-Willstätter-Str. 11, 12489 Berlin, Germany

A. J. Logsdail
Max Planck – Cardiff Centre on the Fundamentals of Heterogeneous Catalysis (FUNCAT), Cardiff Catalysis Institute, School of
Chemistry, Cardiff University, Cardiff CF10 3AT, United Kingdom

J. Strunk
Industrial Chemistry and Heterogeneous Catalysis, Technical University of Munich, Lichtenbergstrße 4, 85748 Garching, Germany

reaction,[11] H_2O_2 synthesis,[12] and alkyne hydrogenation.[13] Considering the continued interest in Pd SACs, it is vital to understand how the binding environment of the Pd sites on such supports affects their charge state, as it frequently correlates with the catalytic activity. Many studies on the Pt SAC systems show that the CO oxidation activity strongly depends on the oxidation state of Pt sites.[14] Knowledge of similar correlations for Pd SACs is thus highly needed.

To obtain comprehensive structural information about the Pd sites on the support (e.g., atomic structure, charge state, coordination type, and number), multiple characterization techniques and theoretical computations are required.[15] Furthermore, the results obtained from experimental and theoretical studies need to be made comparable between methods, or transferable between systems, but this can be challenging.[16] For example, the formal oxidation state is often derived from experimental assignment, and is defined as the degree of oxidation of an atom in terms of counting electrons.[17] Taking PdO as an example, Pd ($4d^{10}$) and O ($2 s^2 2p^4$) bind to form PdO, and the valence octet of O is completed ($2 s^2 p^6$) resulting in an oxidation state of -2, while Pd adopts a $4d^8$ configuration with an oxidation state of $+2$; however, computational analysis using Bader approach, which partition electronic density within a contour of zero density gradient, gives inconsistent results.[18] Indeed, Bader analysis of charge distribution in PdO gives $+0.86$ e for the constituent Pd species. Effort is needed to correlate the computationally derived charge partitioning with the formally derived oxidation state, in a manner similar to that achieved with experiment. Resolving the differences will aid bridging the gap between theory and experiment.

In this work, comprehensive X-ray photoelectron spectroscopy (XPS), X-ray absorption (XAS), and CO-DRIFTS studies are combined with Bader charge analysis to fully understand the electronic and coordination structure of Pd as function of the support: PCN, hexagonal BN (hBN), Si_3N_4, and TiN are used as nitride supports, with corresponding and additional oxide supports (B_2O_3, SiO_2, TiO_2, as well as ZnO and Al_2O_3) for comparison. Upon deposition of Pd with the same procedure, the supports are assumed to be the only factor influencing the electronic and coordination structure of the as-prepared Pd catalysts. The experimental studies, in combination with density functional theory (DFT) calculations, allowed us to identify structure, electronic state and oxidation state and to compare Pd on nitride supports with oxide supports. On the basis of common principles (i.e., electronegativity), the systematic correlations between formal oxidation state, computed Bader charge, stretching frequency of adsorbed CO are investigated.

Results and discussion

Several available commercial supports were selected, PCN was self-synthesized, and their surface areas, ranging from 8 to $168 \, m^2 g^{-1}$, were analyzed via nitrogen physisorption (BET method, see Figure S1). Pd was added by a wet impregnation method using organometallic palladium salts [Pd(TFA)$_2$, Pd(acac)$_2$, and Pd(OAc)$_2$] in acetone (see

Materials and Methods section, Supporting Information). The low-boiling-point and low-polarity solvent acetone prevents Pd agglomeration and results in the atomic dispersion of cationic Pd species.[19] The achievement of the desired Pd loading of about 1 wt % on different supports was confirmed by inductively coupled plasma-optical emission spectroscopy (ICP-OES, Table S1). The successful deposition of Pd was further confirmed by enhanced absorbance in UV-Vis DRS (Figures S2 and S3). The XRD (Figures S4 and S5) and DRIFTS (Figures S6 and S7) measurements on samples before and after Pd deposition proved that the crystal structure and molecular structure of the support materials remain the same in all samples. For the sake of completeness, it must be mentioned that some residual ligand remained in the samples, in particular on the oxide surface, but it is not – at least not strongly – attached to the Pd atoms (see Supplementary Note 1; Tables S2 - S4; Figures S8 - S10 for temperature programmed decomposition, TPDE, of the residual ligand).

By XPS, two types of Pd species were found on all nitride supports (Figure 1 and Figure S11C): One identified by a Pd $3d_{5/2}$ peak at ca. 338.3 eV, and the other one at ca. 336.3 eV. The Pd $3d_{5/2}$ peak positions differ only slightly among the different Pd/nitride samples. The assignment of the peaks was achieved by extensive control experiments with Pd/PCN samples.

Three different Pd(II) salts [Pd(TFA)$_2$, Pd(acac)$_2$, and Pd(OAc)$_2$] were selected for the synthesis of Pd/PCN to investigate a potential influence of the Pd source on the oxidation state of Pd species. Notably, the Pd 3d binding energy in pure Pd(II) salts is slightly different: the Pd $3d_{5/2}$ peaks for Pd(TFA)$_2$, Pd(acac)$_2$, and Pd(OAc)$_2$ are found at 339.1, 338.8, and 338.6 eV, respectively (Figure S11A). However, after anchoring these Pd(II) salts onto PCN with the same synthesis procedure, the resulting Pd species show similar Pd $3d_{5/2}$ binding energies of between 338.1 and 338.3 eV (Figure 1 and Figure S11B), indicating the formation of certain bond between Pd and PCN surface and excluding the influence of the ligands from different precursors (TFA, acac, and OAc).

The loading-dependent study over Pd/PCN samples was conducted, ranging from 0.5 wt % to 16 wt %, and TEM, XAS and XPS measurements were performed. High-angle annular dark-field scanning transmission electron microscopy (HAADF-STEM, Figure S14) showed that Pd speciation is predominantly atomically dispersed in the samples with Pd loading of 0.5 wt % and 2 wt %, with only a very few nanoparticles being observed. In the sample with 16 wt % Pd loading, nanoclusters (~2 nm diameter) are the dominant species. The analysis of the extended X-ray absorption fine structure (EXAFS) Pd K data on this set of samples (Table S5) revealed the formation of long-order Pd structure in the samples with the highest loading, seen as an increase in the intensity of the peaks corresponding to the second scattering shell in Pd metal at 2.49 Å in the Fourier transformed data (Figure 2A). This hints to the formation of the large Pd nanoparticle in agreement with TEM data. Moreover, the position of the white line (Dotted area in Figure 2B) in X-ray absorption near edge structure
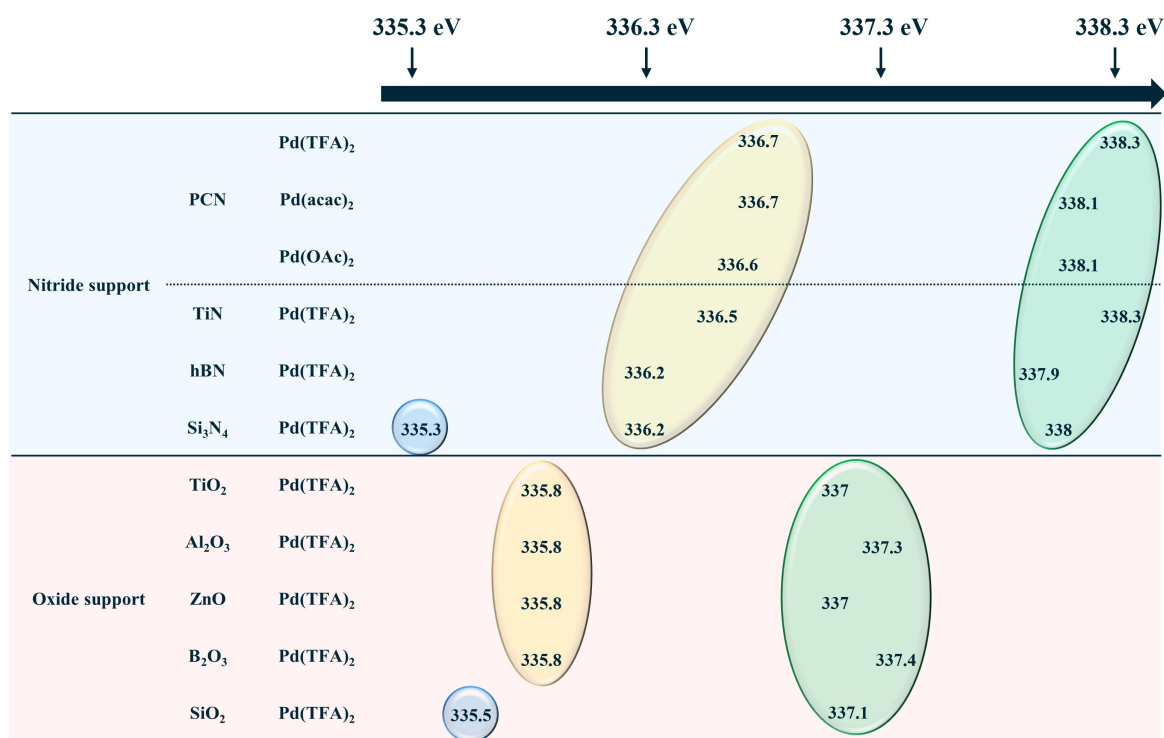
Figure 1. Binding energy of Pd 3d$_{5/2}$ obtained from XPS for various Pd catalysts with 1 wt% loading.
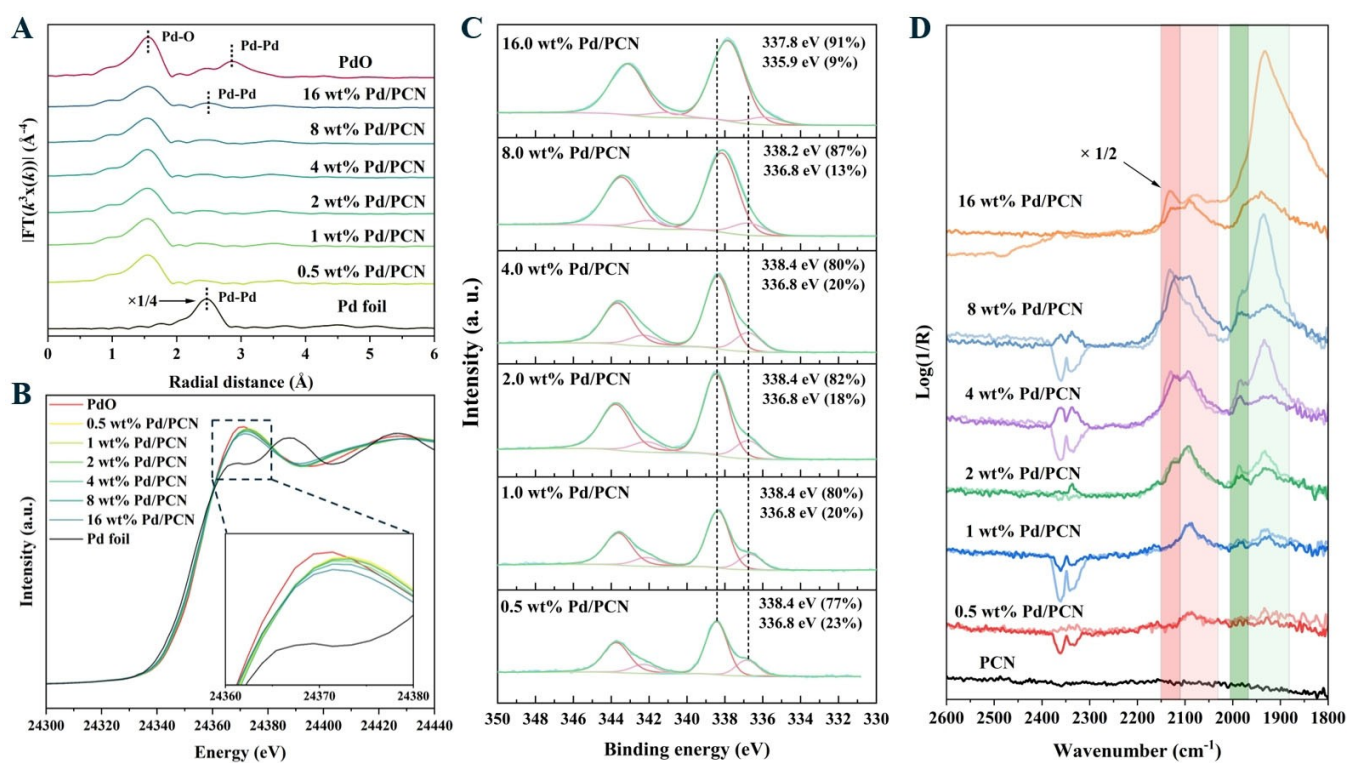
Figure 2. Characterization data of various Pd/PCN samples with different Pd loading: (A) the magnitude of the Fourier transformed k^3-weighted Pd K EXAFS data (not phase corrected), (B) Pd K-edge XANES spectra (the inset shows the enlarged region around the white line maximum), (C) Pd 3d XPS data, and (D) CO-DRIFTS spectra (shown using pale line) and CO-DRIFTS spectra of the washed Pd/PCN samples, shown using intensely colored line.

(XANES) spectra shows gradual negative shift of 2 eV, and its intensity decreased with increase of the Pd loading. The shift of the edge to the lower energies and the decrease in intensities of the white line further hint to a decrease in the Pd oxidation state with increasing Pd loading.

A significant negative shift of the Pd 3d binding energy was also found in the sample with the highest loading of 16 wt % (XPS, Figure 2C), in agreement with Pd K XANES data. Based on these findings, the binding energy of Pd $3d_{5/2}$ of the different Pd species appearing in the Pd/PCN samples can then be assigned as follows: the peak at a binding energy of 338.3 eV corresponds to the atomically dispersed Pd species, the peak at a binding energy of 336.3 eV is attributed to the Pd nanoclusters, and the peak at a binding energy of 335.4 eV, observed in the calcined sample, is assigned to the large Pd nanoparticle (Figure S13).

It is noteworthy that, without any calcination, a third Pd $3d_{5/2}$ peak with a low binding energy of 335.3 eV was observed in Pd/Si_3N_4. The analysis of the EXAFS data on this sample proposed the existence of Pd–O–Si species (Figure 3A). As a similar peak at binding energy of 335.5 eV was observed in XPS spectra for the Pd/SiO_2 sample, these findings hint to the presence of some Si-oxide impurity in Si_3N_4.

For the Pd/oxide samples, two types of Pd species are also observed via XPS, and their Pd 3d binding energies are shifted to lower binding energy compared to those on nitride supports: One is at ca. 337.3 eV, and the second one is at ca. 335.8 eV (Figure 1 and Figure S11D). From the HAADF-STEM images of 1 wt % Pd/TiO_2 (Figure S17), apart from the atomically dispersed Pd species, a large amount of Pd nanoclusters (~2 nm) are observed, which is due to the

aggregation of the residual Pd salts. Upon increasing the Pd loading from 1 wt % to 4 wt %, the relative ratio of Pd species with a low valence state (ca. 335.8 eV) significantly increased (Figure S18A), suggesting the formation of more Pd nanoclusters. A similar trend is observed in the Pd 3d XPS spectra of high-loading 4 wt % Pd/Al_2O_3 (Figure S18B). Therefore, we associated the broad peak at 337 eV with the atomic Pd species, while the component at 335.8 eV was assigned to Pd nanoclusters. One additional peak at a binding energy of 334.3 eV was observed in the 400 °C calcined Pd/TiO_2 samples (Figure S19), which was attributed to the formation of large Pd nanoparticles, as observed from HAADF-STEM (Figure S20). Notably, the Pd 3d peak at binding energies of 334.3 eV in Pd/TiO_2 samples shifted below the corresponding values for Pd foil (335.3 eV).[20] This is due to the strong metal-support effect known for Pd with TiO_2, as indicated by the presence of well-attached nonspherical Pd nanoparticles on the surface of TiO_2 (Figure S20), leading to TiO_2-supported Pd being more electronegative than zero-valent Pd alone.[21]

Further information on the electronic structure of the Pd atom on nitride and oxide supports can be derived from the analysis of XANES data. The shape of the XANES spectra (Figure 3B) for Pd/TiO_2, Pd/Al_2O_3, and Pd/ZnO is close to the bulk PdO. In contrast, differing significantly from the bulk PdO spectra were observed in the Pd/hBN, Pd/Si_3N_4, and Pd/PCN samples (Figure 3B), indicated by a shift of the white line at 24370 eV towards higher energy and an increase in intensity at 24390 eV. This might hint to the distinct coordination environments for Pd on nitride- and oxide-based supports. Additionally, significant modifications in the XANES spectral shape among different Pd/nitride
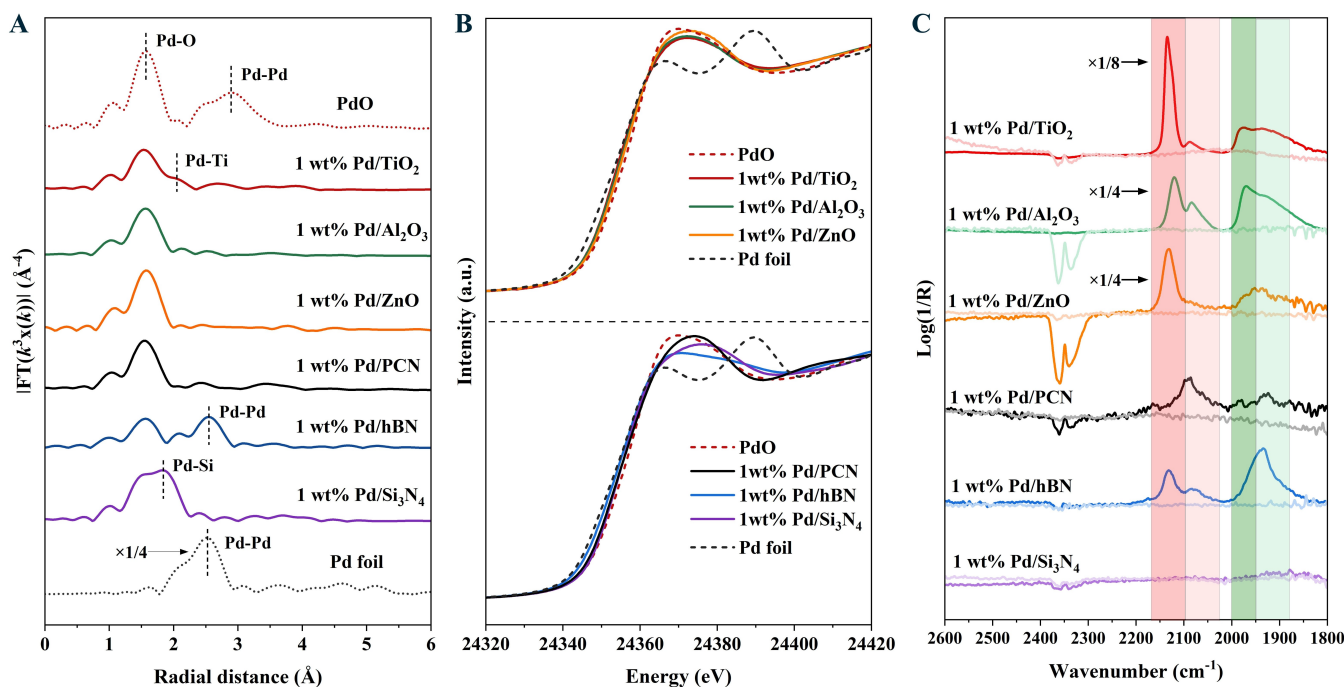
Figure 3. Characterization data of 1 wt % Pd loading on oxide and nitride supports: (A) the magnitude of the Fourier transformed k^3-weighted Pd K EXAFS data (not phase corrected), (B) Pd K-edge XANES spectra, and (C) CO-DRIFTS data.

samples were observed, particularly for the Pd/hBN sample, as its white line intensity dropped significantly. The EXAFS data for the Pd/hBN sample (Figure 3A) show a pronounced peak at about 2.5 Å, which can be attributed to the Pd–Pd coordination shell, confirming the presence of Pd nanoparticle. The EXAFS fitting results are summarized in Supporting Information Tables 5 and 6.

The influence of the support on the oxidation state of Pd was further investigated by CO-DRIFTS. It is known that the stretching frequency of adsorbed CO can probe the charge state of the surface metal species.[3,14a,22] Three selected Pd/nitride samples (Figure 3C) generally showed two types of carbonyl bands, which are related to linear CO on isolated Pd cations and bridged CO on Pd nanoclusters, respectively. No adsorbed CO was present on the bare nitride supports under present experimental conditions. However, the vibrational bands of adsorbed CO for the Pd/nitride samples are weak, up to the point that no signal was observed in 1 wt % Pd/Si$_3$N$_4$. To obtain more pronounced IR response, the Pd/PCN samples with higher loading were studied (Figure 2D), and four sets of bands of adsorbed CO centered at 2123, 2090, 1987, and 1933 cm^{-1} were identified. The IR bands at 2123 and 2090 cm^{-1} were assigned to CO linearly adsorbed on isolated Pd atoms with different oxidation state.[20c,23] The IR bands centered at 1987 and 1933 cm^{-1} were assigned to bridged CO on the Pd nanoclusters.[24] This assignment was further confirmed by the CO-DRIFTS measurement of Pd(TFA)$_2$ (Figure S21), which exhibits a distinct bridge-bound carbonyl band centered at 1969 cm^{-1}. Besides, the Pd(TFA)$_2$ shows no infrared bands of adsorbed CO in the region of 2050–2130 cm^{-1}. This confirms that the bands observed at 2123 and 2090 cm^{-1} in Pd/PCN are derived from CO adsorbed on anchored Pd sites, rather than from the Pd precursor. Notably, a linear CO adsorption sequence on different Pd sites was further observed. The Pd/PCN samples below 1 wt % loading have only one band of linear adsorption, centered at 2090 cm^{-1}, corresponding to the Pd species with a low binding energy in XPS. With the Pd loading increased to 2 wt %, the intensity of the IR band centered at 2090 cm^{-1} remains the same, suggesting the saturation of this type of Pd species. At the same time, a new vibrational band of linearly adsorbed CO centered at 2123 cm^{-1} emerged, suggesting the presence of another Pd species, and its intensity rises to saturation when the Pd loading is increased to 4 wt %. Further increasing Pd loading will only contribute to the bridge carbonyl signal at 1987 and 1933 cm^{-1}, suggesting the formation of more Pd nanoclusters.

To sum up the results of XPS and CO-DRIFT measurements, a Pd anchoring sequence on PCN was observed: (1) cationic Pd with a low oxidation state with an adsorbed CO stretching frequency of 2090 cm^{-1}, (2) cationic Pd with a high oxidation state with adsorbed CO stretching frequency of 2123 cm^{-1}, and (3) partially oxidized Pd sites with two CO stretching frequencies centered at 1987 and 1933 cm^{-1}, respectively. From the Pd 3d XPS spectra, however, only two types of Pd species were observed. Therefore, it is reasonable to assume that the peak at the binding energy of 338.3 eV may contain at least two types of Pd species: one is a Pd species bound to the PCN support, and the other one comprises loosely bound Pd species, i.e. Pd salts.

In comparison to Pd/nitride samples, sharper carbonyl bands were observed for all three Pd/oxide samples. For Pd/TiO$_2$, the CO vibrational bands at 2135 and 2126 cm^{-1} are attributed to CO adsorbed on isolated Pd species with different oxidation state, whereas the vibrational band at 2088 cm^{-1} is attributed to CO linearly adsorbed on either the Pd nanoclusters or Pd–Ti species, as found from EXAFS fitting (Figure 3A). The broad bands centered at 1969 and 1938 cm^{-1} are assigned to bridge-bound carbonyl on Pd nanoclusters that are formed due to the aggregation of loosely bound Pd salts.[20c,25] When increasing the Pd loading to 4 wt %, the band intensity for linear carbonyl at 2135 and 2126 cm^{-1} remains the same, but the band intensity for bridged carbonyl at 1938 cm^{-1} significantly enhanced, confirming the increase in the amount of Pd nanoclusters (Figure S18C). A similar trend was found after comparison of the CO-DRIFT spectrum of 1 wt % and 4 wt % Pd/Al$_2$O$_3$ (Figure S18D). The formation of more Pd nanoclusters in 4 wt % Pd/TiO$_2$ and 4 wt % Pd/Al$_2$O$_3$ agrees well with the observation from their Pd 3d XPS spectra (Figure S18). Moreover, for Pd/TiO$_2$, a CO oxidation sequence on different Pd species was observed: the CO molecules adsorbed on Pd nanoclusters were quickly oxidized and removed upon O$_2$ exposure at 25 °C, as indicated by the rapid drop in the major CO bands at 1969 and 1938 cm^{-1} (Figure S22); afterward, the bands related to linearly adsorbed CO on Pd, with signals at 2088, 2126, and 2135 cm^{-1}, were oxidized in this order with the increased temperature to 200 °C. A similar CO oxidation sequence was also observed in Pd/Al$_2$O$_3$ (Figure S23) and Pd/ZnO (Figure S24).[26] These results show that the CO binding strength broadly follow the trend of the Pd oxidation state: the stronger bonding of CO molecules to Pd species when Pd compounds are more oxidized. Besides, a CO-induced Pd sintering was observed in the Pd/TiO$_2$ sample (Figure S25), as further confirmed by NAP-XPS. The NAP-XPS spectrum of the Pd 3d core line (Figure S26) reveals that the isolated Pd species (~337.4 eV) turned into near-neutral Pd$^{\delta+}$ species (~336.2 eV) after CO adsorption, where the formation of a stable carbonyl weakens the interaction of Pd atom to support.[3]

The experimentally gained information was used to benchmark the theoretical calculation. We applied Bader charge analysis to compute the effective charge of the Pd sites for all candidate Pd/PCN and Pd/TiO$_2$ models (Tables S7 and S8). However, some discrepancies arose when assigning the candidate models to different oxidation states. For example, the Bader charge of (PdN$_4$)$_{surface}$ model is +0.82 e (Figure S30), and the value for the (PdN$_4$)$_{interlayer}$ model is +0.51 e (Figure S31), while both models are fitted with a coordination number of 4 in the FT-EXAFS fitting (Table S6). Notably, the EXAFS-fitted coordination numbers need to be considered with care in the model assignment, i.e.,the EXAFS-derived coordination number is an average result of all atoms.[27] Hence, it cannot accurately reflect the coordination structure when the samples are heterogeneous, e.g., upon co-existence of atomically dispersed species and nanoclusters in the Pd/TiO$_2$ sample.

Therefore, we propose using the oxidation state as an additional calibration standard for the model assignments.

First, to Figure out the relationship between the formal oxidation state and computed Bader charge, we selected a series of Pd–C, Pd–N, Pd–O, and Pd–F models with different oxidation states ($+1$, $+2$, $+3$, and $+4$) and then calculated their respective Bader charges. A correlation analysis was performed between the Bader charge of Pd and the corresponding Allen electronegativity of the coordinating anions (C, N, O, and F), and four linear equations were obtained (Figure 4A). These linear relationships are reasonable because the electronegativity of anions increases from carbon to fluorine across the periodic table,[28] which is reflected in the changes of the Bader charge of the cation. For reference, four additional Pd^{2+} models (Pd–4C, Pd–4S, Pd–4N and Pd–4O, Figure S27) were studied, and a similar equation was obtained, well confirming the above relationship between Bader charge and electronegativity.

Next, we correlated the Bader charge with the oxidation state (Figure 4B). For all Pd models, however, the tendency is more like a parabolic relationship rather than a linear relationship, with the most linear-like dependence for Pd–C models. With the systematic correlations and equations thus obtained for Pd–N and Pd–O models, the oxidation state of the differently coordinated Pd sites in the Pd/PCN and Pd/TiO$_2$ models can be obtained based on the corresponding Bader charges, as listed in Tables S7 and S8, respectively. These results indicated that the Pd oxidation state depends strongly on the type and number of coordinating anions. More importantly, the above relationship provides a way to directly assign the formal oxidation state to the Pd site in the candidate models, allowing us to match it with the experimental oxidation state data and to determine an appropriate theoretical model.

We now turn to the relationship between the CO stretching frequency and oxidation state of the isolated Pd species. As shown in Figures 4C and 4D, the stretching frequency of CO is proportional to the oxidation state of isolated Pd species for both Pd/PCN models and Pd/TiO$_2$ models. Combining the relation equation between Bader charge and oxidation state (Figure 4B) with the relation equation between Bader charge and CO stretching frequency (Figures 4C and 4D), two separate equations

$$Nu_{CO} = 1981 + 45.4x - 2.06x^2 \tag{1}$$

$$Nu_{CO} = 2001 + 55.6x - 3.50x^2 \tag{2}$$

can be introduced for Pd/PCN and Pd/TiO$_2$, respectively. Nu_{CO} (cm^{-1}) is the experimental CO stretching frequency, x is the corresponding oxidation state of Pd, and a difference of 9 cm^{-1} between the experimental (2143 cm^{-1}) and computational (2134 cm^{-1}) CO stretching frequency was taken into account in the equations. With the stretching frequency of adsorbed CO known from the DRIFTS experiment, equations (1) and (2) can be used to estimate the oxidation state of Pd on PCN and TiO$_2$, respectively. As shown in Table S9, the calculated oxidation state of Pd on the PCN support is higher than that on the TiO$_2$ support, in agreement with the

above XPS data (Figure 1). For Pd/PCN, based on the calculated oxidation state of 3.77 and the measured coordination number of 4, it is proposed that the (PdN$_4$)$_{surface}$ model (Figure 4C) is most appropriate, in which Pd binds to four surface nitrogen atoms. The Pd species with a calculated oxidation state of 2.84 can be assigned to the model (PdN$_3$)$_{surface}$, where the Pd atom is bound to three N atoms on the surface. In this respect, the combination of the stretching frequency of adsorbed CO, the experimental coordination information, and the calculated oxidation state allows for the distinction between different surface Pd species.[3,29]

Notably, the hydroxyl group cannot be ignored on the oxide surface.[30] The excess hydroxyl group would coordinate with Pd atoms through M–O(OH) (metal–hydroxyl group) interactions. Therefore, for Pd/TiO$_2$, the Pd species with a calculated oxidation state of 2.99 is assigned to the Pd(OH)$_2$ model (Figure 4D), where the Pd atom is bound to one lattice O and two extra –OH groups on the surface, and the Pd species with a calculated oxidation state of 1.75 is attributed to the PdOH model, where the Pd atom is bound to one lattice O and one extra –OH group on the surface. The proposed Pd structures have calculated oxidation states of $+2.1$ for the Pd(OH)$_2$ model, and $+1.2$ for the PdOH model. The calculated oxidation state of the assigned model agrees with experimental observations from the Pd 3d XPS results.

Conclusions

With systematic studies of dedicated sample series and the extensive experimental and computational characterization, three important findings were obtained: (1) It was shown that the oxidation state of Pd on nitride supports is higher than on oxide supports. This was attributed to the existence of Pd in distinct local coordination environments (Pd–N$_x$ on nitride and Pd–(OH)$_x$ on oxide); (2) Systematic correlations between Bader charge, electronegativity, vibrational frequency of adsorbed CO and chemical oxidation have been obtained for both types of support; (3) the aforementioned correlations allowed to choose the correct computational model for the coordination structure of Pd to the surface. It must be specifically noted that the combined methodology presented here allows distinguishing more accurately between atomically dispersed Pd, residual precursor, and nanoclusters. Hence, it may not be required to prepare samples containing exclusively only one type of Pd species. We are convinced that our findings will significantly contribute to the further understanding of metal-support interactions in heterogeneous catalysis, and lead to a systematic development of catalysts for specific purposes.

Angew. Chem. Int. Ed. **2024**, e202400174 (6 of 9)

© 2024 The Authors. Angewandte Chemie International Edition published by Wiley-VCH GmbH
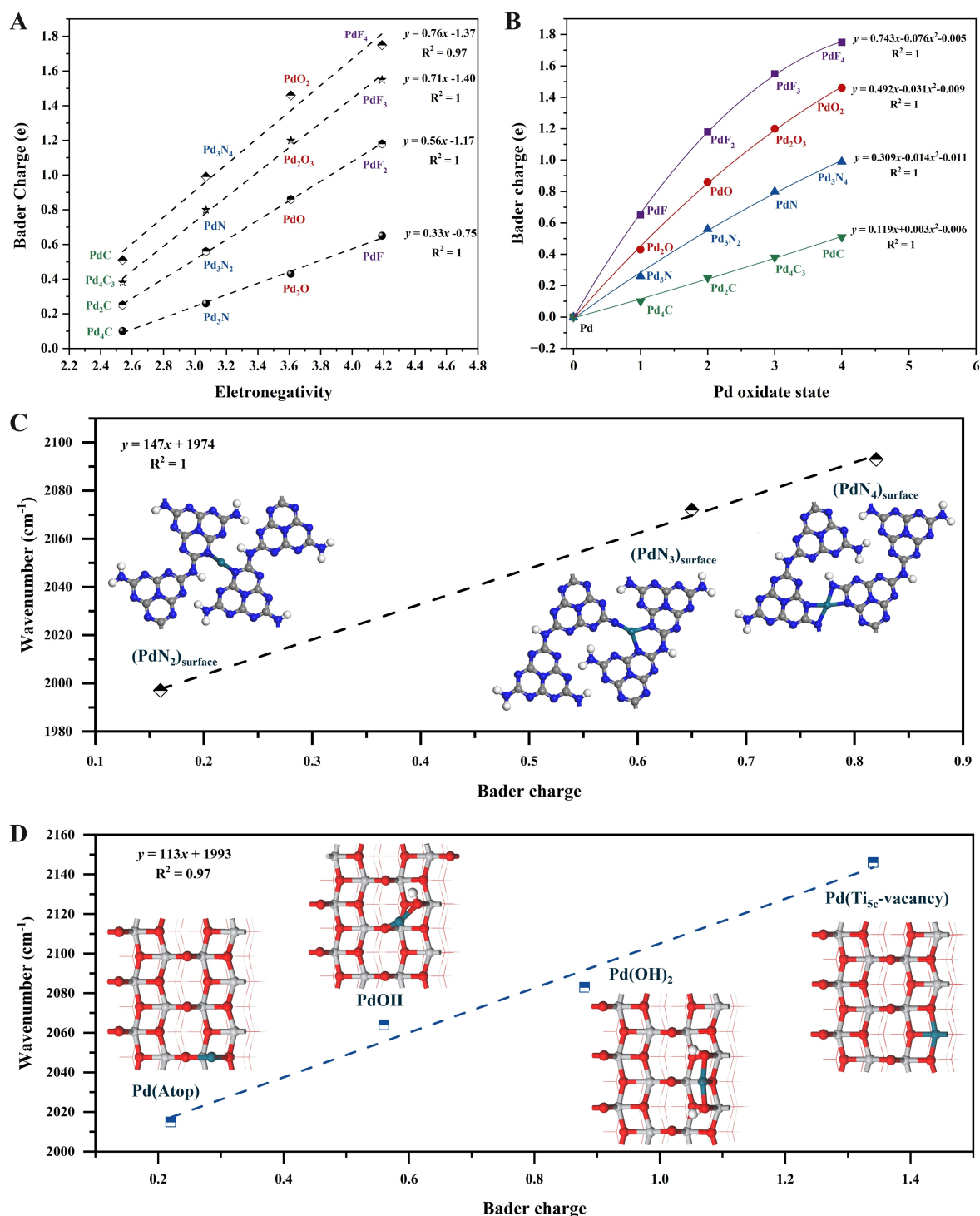
Figure 4. (A) Bader charge for Pd models with different oxidation state ($+1$, $+2$, $+3$, and $+4$), plotted against the electronegativity of different type of bonding atom (C, N, O, and F). (B) Bader charge-oxidation state plots for different Pd models. (C and D) Plots of Bader charge and CO stretching frequency for Pd/PCN model and Pd/TiO$_2$(101) model, respectively. Pd, C, N, H, Ti, O atoms are dark green, grey, blue, white, light-grey, and red spheres, respectively.

Angew. Chem. Int. Ed. **2024**, e202400174 (7 of 9)

© 2024 The Authors. Angewandte Chemie International Edition published by Wiley-VCH GmbH

Conflict of Interest

The authors declare no conflict of interest.

Data Availability Statement

The data that support the findings of this study are available from the corresponding author upon reasonable request.

[1] a) X. Cui, W. Li, P. Ryabchuk, K. Junge, M. Beller, *Nature Catalysis* **2018**, *1*, 385–397; b) B. B. Sarma, F. Maurer, D. E. Doronkin, J. D. Grunwaldt, *Chem. Rev.* **2022**, *123*, 379–444.

[2] V. Muravev, A. Parastaev, Y. van den Bosch, B. Ligt, N. Claes, S. Bals, N. Kosinov, E. J. M. Hensen, *Science* **2023**, *380*, 1174–1178.

[3] J. Hulva, M. Meier, R. Bliem, Z. Jakub, F. Kraushofer, M. Schmid, U. Diebold, C. Franchini, G. S. Parkinson, *Science* **2021**, *371*, 375–379.

[4] a) L. Nie, D. Mei, H. Xiong, B. Peng, Z. Ren, X. I. P. Hernandez, A. DeLaRiva, M. Wang, M. H. Engelhard, L. Kovarik, A. K. Datye, Y. Wang, *Science* **2017**, *358*, 1419–1423; b) Z. Teng, Q. Zhang, H. Yang, K. Kato, W. Yang, Y.-R. Lu, S. Liu, C. Wang, A. Yamakata, C. Su, B. Liu, T. Ohno, *Nature Catalysis* **2021**, *4*, 374–384; c) H. Zhang, S. Zuo, M. Qiu, S. Wang, Y. Zhang, J. Zhang, X. W. D. Lou, *Sci. Adv.* **2020**, *6*, eabb9823; d) L. Luo, J. Luo, H. Li, F. Ren, Y. Zhang, A. Liu, W. X. Li, J. Zeng, *Nat. Commun.* **2021**, *12*, 1218.

[5] a) N. C. Nelson, L. Chen, D. Meira, L. Kovarik, J. Szanyi, *Angew. Chem. Int. Ed.* **2020**, *59*, 17657–17663; b) L. Chen, S. I. Allec, M. T. Nguyen, L. Kovarik, A. S. Hoffman, J. Hong, D. Meira, H. Shi, S. R. Bare, V. A. Glezakou, R. Rousseau, J. Szanyi, *J. Am. Chem. Soc.* **2023**, *145*, 10847–10860.

[6] a) K. Fujiwara, S. E. Pratsinis, *AIChE J.* **2016**, *63*, 139–146; b) K. Fujiwara, S. E. Pratsinis, *Appl. Catal. B* **2018**, *226*, 127–134.

[7] Z. Wang, D. Ren, Y. He, M. Hong, Y. Bai, A. Jia, X. Liu, C. Tang, P. Gong, X. Liu, W. Huang, Z. Zhang, *ACS Catal.* **2023**, *13*, 10056–10064.

[8] a) R. Lang, X. Du, Y. Huang, X. Jiang, Q. Zhang, Y. Guo, K. Liu, B. Qiao, A. Wang, T. Zhang, *Chem. Rev.* **2020**, *120*, 11986–12043; b) Y. Kim, G. Collinge, M. S. Lee, K. Khivantsev, S. J. Cho, V. A. Glezakou, R. Rousseau, J. Szanyi, J. H. Kwak, *Angew. Chem. Int. Ed.* **2021**, *60*, 22769–22775.

[9] F. Maurer, J. Jelic, J. J. Wang, A. Ganzler, P. Dolcet, C. Woll, Y. M. Wang, F. Studt, M. Casapu, J. D. Grunwaldt, *Nature Catalysis* **2020**, *3*, 824–833.

[10] a) J. Gu, C. S. Hsu, L. Bai, H. M. Chen, X. Hu, *Science* **2019**, *364*, 1091–1094; b) H. Fei, J. Dong, Y. Feng, C. S. Allen, C. Wan, B. Volosskiy, M. Li, Z. Zhao, Y. Wang, H. Sun, P. An, W. Chen, Z. Guo, C. Lee, D. Chen, I. Shakir, M. Liu, T. Hu, Y. Li, A. I. Kirkland, X. Duan, Y. Huang, *Nature Catalysis* **2018**, *1*, 63–72; c) Z. Li, Y. Chen, S. Ji, Y. Tang, W. Chen, A. Li, J. Zhao, Y. Xiong, Y. Wu, Y. Gong, T. Yao, W. Liu, L. Zheng, J. Dong, Y. Wang, Z. Zhuang, W. Xing, C.-T. He, C. Peng, W.-C. Cheong, Q. Li, M. Zhang, Z. Chen, N. Fu, X. Gao, W. Zhu, J. Wan, J. Zhang, L. Gu, S. Wei, P. Hu, J. Luo, J. Li, C. Chen, Q. Peng, X. Duan, Y. Huang, X.-M. Chen, D. Wang, Y. Li, *Nat. Chem.* **2020**, *12*, 764–772; d) W. Liu, L. Zhang, W. Yan, X. Liu, X. Yang, S. Miao, W. Wang, A. Wang, T. Zhang, *Chem. Sci.* **2016**, *7*, 5758–5764; e) S. Buchele, Z. Chen, E. Fako, F. Krumeich, R. Hauert, O. V. Safonova, N. Lopez, S. Mitchell, J. Perez-Ramirez, *Angew. Chem. Int. Ed.* **2020**, *59*, 19639–19644.

[11] Z. Chen, E. Vorobyeva, S. Mitchell, E. Fako, M. A. Ortuno, N. Lopez, S. M. Collins, P. A. Midgley, S. Richard, G. Vile, J. Perez-Ramirez, *Nat. Nanotechnol.* **2018**, *13*, 702–707.

[12] R. Arrigo, M. E. Schuster, S. Abate, G. Giorgianni, G. Centi, S. Perathoner, S. Wrabetz, V. Pfeifer, M. Antonietti, R. Schlögl, *ACS Catal.* **2016**, *6*, 6959–6966.

[13] G. Vile, D. Albani, M. Nachtegaal, Z. Chen, D. Dontsova, M. Antonietti, N. Lopez, J. Perez-Ramirez, *Angew. Chem. Int. Ed.* **2015**, *54*, 11265–11269.

[14] a) L. DeRita, J. Resasco, S. Dai, A. Boubnov, H. V. Thang, A. S. Hoffman, I. Ro, G. W. Graham, S. R. Bare, G. Pacchioni, X. Pan, P. Christopher, *Nat. Mater.* **2019**, *18*, 746–751; b) B. Qiao, A. Wang, X. Yang, L. F. Allard, Z. Jiang, Y. Cui, J. Liu, J. Li, T. Zhang, *Nat. Chem.* **2011**, *3*, 634–641; c) H. Jeong, D. Shin, B. S. Kim, J. Bae, S. Shin, C. Choe, J. W. Han, H. Lee, *Angew. Chem. Int. Ed.* **2020**, *59*, 20691–20696.

[15] a) A. G. Melike Babucci, B. C. Gates, *Chem. Rev.* **2020**, *120*, 11956–11985; b) X. C. Lulu Li, X. Lin, Z.-J. Zhao, J. Gong, *Chem. Soc. Rev.* **2020**, *49*, 8156–8178.

[16] A. Walsh, A. A. Sokol, J. Buckeridge, D. O. Scanlon, C. R. A. Catlow, *Nat. Mater.* **2018**, *17*, 958–964.

[17] *The IUPAC Compendium of Chemical Terminology, 2nd ed.* (Eds.: A. D. McNaught, A. Wilkinson), Blackwell Scientific Publications, Oxford, **1997**.

[18] a) R. F. W. Bader, *Acc. Chem. Res.* **1985**, *18*, 9–15; b) W. Tang, E. Sanville, G. Henkelman, *J. Phys. Condens. Matter* **2009**, *21*, 084204.

[19] X. Sun, S. R. Dawson, T. E. Parmentier, G. Malta, T. E. Davies, Q. He, L. Lu, D. J. Morgan, N. Carthey, P. Johnston, S. A. Kondrat, S. J. Freakley, C. J. Kiely, G. J. Hutchings, *Nat. Chem.* **2020**, *12*, 560–567.

[20] a) C. Dong, Z. Gao, Y. Li, M. Peng, M. Wang, Y. Xu, C. Li, M. Xu, Y. Deng, X. Qin, F. Huang, X. Wei, Y.-G. Wang, H. Liu, W. Zhou, D. Ma, *Nature Catalysis* **2022**, *5*, 485–493; b) D. Wu, W. Baaziz, B. Gu, M. Marinova, W. Y. Hernández, W. Zhou, E. I. Vovk, O. Ersen, O. V. Safonova, A. Addad, N. Nuns, A. Y. Khodakov, V. V. Ordomsky, *Nature Catalysis* **2021**, *4*, 595–606; c) V. Muravev, G. Spezzati, Y.-Q. Su, A. Parastaev, F.-K. Chiang, A. Longo, C. Escudero, N. Kosinov, E. J. M. Hensen, *Nature Catalysis* **2021**, *4*, 469–478.

[21] R. F. H. T. H. Fleisch, A. T. Bell, *J. Catal.* **1983**, *87*, 398–413.

[22] a) K. Ding, A. Gulec, A. M. Johnson, N. M. Schweitzer, G. D. Stucky, L. D. Marks, P. C. Stair, *Science* **2015**, *350*, 189–192; b) H. V. Thang, G. Pacchioni, L. DeRita, P. Christopher, *J. Catal.* **2018**, *367*, 104–114.

[23] F. C. Meunier, *J. Phys. Chem. C* **2021**, *125*, 21810–21823.

[24] a) B. B. Sarma, J. Jelic, D. Neukum, D. E. Doronkin, X. Huang, F. Studt, J.-D. Grunwaldt, *J. Phys. Chem. C* **2023**, *127*,

3032–3046; b) I. Jbir, J. Couble, S. Khaddar-Zine, Z. Ksibi, F. Meunier, D. Bianchi, *ACS Catal.* **2016**, *6*, 2545–2558.

[25] V. Muravev, J. F. M. Simons, A. Parastaev, M. A. Verheijen, J. J. C. Struijs, N. Kosinov, E. J. M. Hensen, *Angew. Chem. Int. Ed.* **2022**, *61*, e202200434.

[26] a) R. Naumann d'Alnoncourt, M. Friedrich, E. Kunkes, D. Rosenthal, F. Girgsdies, B. Zhang, L. Shao, M. Schuster, M. Behrens, R. Schlögl, *J. Catal.* **2014**, *317*, 220–228; b) P. Kast, M. Friedrich, D. Teschner, F. Girgsdies, T. Lunkenbein, R. Naumann d'Alnoncourt, M. Behrens, R. Schlögl, *Appl. Catal. A* **2015**, *502*, 8–17.

[27] a) J. Finzel, K. M. Sanroman Gutierrez, A. S. Hoffman, J. Resasco, P. Christopher, S. R. Bare, *ACS Catal.* **2023**, *13*, 6462–6473; b) K. Feng, H. Zhang, J. Gao, J. Xu, Y. Dong, Z. Kang, J. Zhong, *Appl. Phys. Lett.* **2020**, *116*, 191903; c) L. Liu, A. Corma, *Nature Catalysis* **2021**, *4*, 453–456.

[28] a) L. C. Allen, *J. Am. Chem. Soc.* **1989**, *111*, 9003–9014; b) T. L. M. J. B. Mann, L. C. Allen, *J. Am. Chem. Soc.* **2000**, *122*, 2780–2783; c) T. L. M. J. B. Mann, E. T. Knight, J. F. Capitani, L. C. Allen, *J. Am. Chem. Soc.* **2000**, *122*, 5132–5137.

[29] H. A. Aleksandrov, K. M. Neyman, K. I. Hadjiivanov, G. N. Vayssilov, *Phys. Chem. Chem. Phys.* **2016**, *18*, 22108–22121.

[30] a) M. Wagner, B. Meyer, M. Setvin, M. Schmid, U. Diebold, *Nature* **2021**, *592*, 722–725; b) J. Saavedra, H. A. Doan, C. J. Pursell, L. C. Grabow, B. D. Chandler, *Science* **2014**, *345*, 1599–1602; c) S. Cao, Y. Zhao, S. Lee, S. Yang, J. Liu, G. Giannakakis, M. Li, M. Ouyang, D. Wang, E. C. H. Sykes, M. Flytzani-Stephanopoulos, *Sci. Adv.* **2020**, *6*, eaba3809.

Research Articles

Heterogeneous Catalysis

J. Huang, M. Klahn, X. Tian, S. Bartling,
A. Zimina, M. Radtke, N. Rockstroh,
P. Naliwajko, N. Steinfeldt, T. Peppel, J.-
D. Grunwaldt, A. J. Logsdail, H. Jiao,
J. Strunk* ——————— **e202400174**

Fundamental Structural and Electronic
Understanding of Palladium Catalysts on
Nitride and Oxide Supports
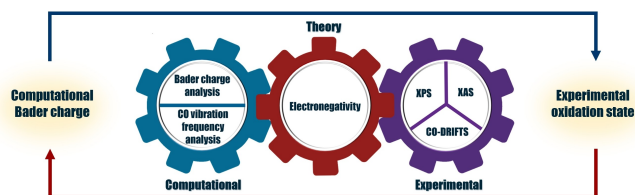
The effect of the support type (nitride and oxide) on the charge state of isolated Pd sites has been explored in this work. Furthermore, a correlation was established between the formal oxidation state, the vibrational frequency of adsorbed CO, and the computed Bader charge based on the periodic trends in electronegativity, allowing the identification of appropriate models for the understanding of the coordination structure of Pd center.